macromol

MDPI

Article

Construction of Superhydrophobic Surfaces Enhanced by Silanized-CNC-Assisted PVDF/PDMS Microsphere Coating

Jie Jian [1], Tao Song [1,*], Tingting Han [2] and Alain Dufresne [3]

[1] State Key Laboratory of Advanced Papermaking and Paper-Based Materials, South China University of Technology, Guangzhou 510640, China; 202521029103@mail.scut.edu.cn
[2] Guangzhou Key Laboratory of Sensing Materials & Devices, Centre for Advanced Analytical Science, School of Chemistry and Chemical Engineering, Guangzhou University, Guangzhou 510006, China; tinghan@gzhu.edu.cn
[3] Université Grenoble Alpes, CNRS, Grenoble INP, LGP2, F-38000 Grenoble, France; alain.dufresne@pagora.grenoble-inp.fr
* Correspondence: songt@scut.edu.cn

Abstract

Coatings based on polyvinylidene fluoride (PVDF) and poly(dimethylsiloxane) (PDMS)-based polymeric microspheres can be easily fabricated via non-solvent-induced phase separation (NIPS) and electrostatic spraying (ES) techniques. Both techniques are promising strategies for constructing superhydrophobic surfaces on various substrates. However, PVDF and PDMS inherently suffer from severe aggregation, which generates oversized particles and inhomogeneous microstructures. Conventionally, costly and environmentally hazardous dispersants are required to alleviate this issue, severely restricting the industrial scalability and practical application of such coatings. In this work, methyltrimethoxysilane-modified cellulose nanocrystals (Si-CNCs) were introduced as a green multifunctional modifier to tackle these issues. The results revealed that as structural building blocks and dispersants, Si-CNCs inhibited polymer aggregation via electrostatic repulsion and steric hindrance, refined the particle size and formed uniform micro/nano hierarchical structures. Increasing Si-CNC loading further improved polymer dispersion and superhydrophobic performance. Coatings fabricated by ES showed better hydrophobicity than those fabricated by NIPS. ES achieved a water contact angle (WCA) of 160–166° and a sliding angle (SA) near 1° on cotton fabric, while NIPS had a WCA of 153.8–158° and an SA of around 2°. Wood and glass substrates also obtained favorable superhydrophobicity, with WCAs above 150° and SAs below 1°. Furthermore, all modified surfaces exhibited excellent abrasion resistance. This work provides a relatively eco-friendly, environmentally sustainable, scalable and substrate-flexible strategy for fabricating high-performance PVDF/PDMS-based superhydrophobic coatings.

Keywords: cellulose nanocrystals; superhydrophobicity; non-solvent-induced phase separation; electrostatic spraying

Check for updates

Academic Editors: Luis Alves, Jose Miguel Gonzalez-Dominguez, Albert Nguyen Van Nhien, Caroline Hadad, Víctor Calvo and María Emilia Cano

Received: 21 June 2026
Revised: 4 August 2026
Accepted: 17 August 2026
Published: 19 August 2026

Copyright: © 2026 by the authors. Licensee MDPI, Basel, Switzerland. This article is an open access article distributed under the terms and conditions of the Creative Commons Attribution (CC BY) license.

1. Introduction

Inspired by the self-cleaning effect of lotus leaves and water repellency of butterfly wings, superhydrophobic materials have become one of the key research frontiers within materials science, chemical engineering and environmental remediation. Featuring versatile functions, including self-cleaning [1–4], anti-corrosion [5,6], anti-fogging [7–10] and high-efficiency oil/water separation [11–13], these materials have attracted extensive attention

worldwide in both academia and industry, and hold great application potential in numerous fields, such as medical protection, intelligent transportation, aerospace component protection, oily wastewater treatment, marine antifouling and anti-icing systems, to name only a few [14–19]. It is well recognized that high-performance, durable superhydrophobic surfaces highly rely on the synergistic combination of low-surface-energy compositions and elaborately constructed micro/nanoscale hierarchical roughness, both of which are indispensable [20].

Among the low-surface-energy polymers, polyvinylidene fluoride (PVDF) and polydimethylsiloxane (PDMS) are the most widely used for fundamental research and industrial fabrication of superhydrophobic materials owning to their low surface energy, superior chemical inertness and long-term environmental stability under harsh conditions. Specifically, PDMS is a polymeric material featuring a low surface energy, low density, high optical transparency, excellent thermal resistance over a wide temperature range, and favorable chemical stability. Benefiting from its relatively high viscosity, good mechanical flexibility and biocompatibility, PDMS can anchor micro/nanoparticles onto substrates while reducing the surface energy of the underlying material, thereby enhancing the hydrophobicity and abrasion resistance of coatings [21,22]. On the other hand, PVDF is a highly inert thermoplastic polymer with an outstanding anti-aging capacity, extreme temperature tolerance and ultraviolet resistance. It has been widely adopted for manufacturing corrosion-resistant sealing components, capacitors, insulating materials and ion-exchange membranes. As another low-surface-energy polymer with stable chemical properties, PVDF can contribute to surface roughness and offers a superior weather resistance and mechanical strength [23]. However, the sole use of PVDF or PDMS often fails to achieve long-term stable immobilization of micro/nanoparticles on substrate surfaces. Thus, technically, these polymers are commonly mixed with different micro/nanoparticles to build hierarchical rough structures, endowing coatings with improved hydrophobicity, roughness, abrasion resistance, substrate adhesion, weatherability and mechanical strength via different coating methods [24–26]. Widely adopted micro/nanoparticles include zeolitic imidazolate framework-8 (ZIF-8) [27], nano-TiO_2 [28,29], nano-ZnO [30], SiO_2 [31], polydopamine nanoparticles [32], and so forth. The combination of PVDF/PDMS with these micro/nanoparticles enables the fabrication of superhydrophobic surfaces with targeted functionalities, such as anti-icing, antifouling, anticorrosion and continuous oil–water separation. Unfortunately, most of these micro/nanofillers suffer from complicated synthesis procedures, relatively high costs, and poor compatibility with polymer matrices, which hinder their further industrial translation.

Among the various methods, non-solvent-induced phase separation (NIPS) [33,34] and electrostatic spraying (ES) [35] are regarded as the two most promising scalable techniques for industrial production, due to their simple operation, mild conditions, wide substrate adaptability and feasibility for large-scale continuous fabrication. However, during material preparation via NIPS or ES, PVDF and PDMS molecular chains tend to entangle and aggregate severely, forming oversized particles with an uneven distribution. This phenomenon prevents the formation of uniform and stable micro/nano rough surface, and consequently deteriorates superhydrophobic performance, with a degraded water contact angle stability, increased sliding angle and reduced abrasion resistance [36]. This has become a key technical challenge that hinders their further industrialization and commercialization. In order to overcome the dispersion problem, conventional additives such as nano-SiO_2 [37], metal–organic frameworks (MOFs) [38] and γ-aminopropyltriethoxysilane (KH550) [39] have been adopted. However, MOFs suffer from a high cost and complicated synthesis, while nano-SiO_2 requires energy-intensive high-temperature calcination, and KH550 releases irritating and toxic gases, raising environmental and biological concerns.

Moreover, most existing studies focus on intrinsically hydrophobic films like PVDF and polyethylene, which show poor compatibility with common non-hydrophobic substrates including cotton fabric, wood, glass, metals and ceramics, further limiting practical applications. Therefore, there is an urgent need to develop low-cost, environmentally friendly and high-performance nanofillers that can construct micro/nanoscale roughness, suppress polymer aggregation and achieve a uniform dispersion on diverse substrates.

As an eco-friendly nanomaterial extracted from lignocellulosic biomass, nanocellulose integrates the inherent advantages of natural cellulose, including abundant raw resources, low cost, excellent biodegradability and non-toxicity. Meanwhile, it possesses distinctive nanoscale characteristics, with diameters ranging from 2 to 50 nm, an ultrahigh mechanical modulus of over 100 GPa, a large specific surface area exceeding 200 m^2/g, and a high number of hydroxyl groups distributed on its surface [24,40–44]. It has recently been reported that the morphology, surface charge density, aspect ratio and hydroxyl substitution degree of nanocellulose can effectively modulate its dispersion behavior in solvents. In particular, negatively charged cellulose nanocrystals (CNCs), fabricated via acid hydrolysis or TEMPO-mediated oxidation [26,45,46], can inhibit the aggregation of polymer and nanoparticles through the combined effects of spatial confinement, hydrogen bonding and electrostatic repulsion, enabling the fabrication of a uniform dispersing system [24–26,47–51]. In addition, the biodegradability of nanocellulose avoids residual pollution caused by traditional fluorinated superhydrophobic materials, supporting green and low-cost material development. Nevertheless, abundant surface hydroxyl groups endow pristine cellulose with strong hydrophilicity, which restricts its direct application in superhydrophobic systems. Accordingly, hydrophobic modification is required to tackle this challenge by grafting hydrophobic moieties onto CNC surfaces to reduce surface energy. Among diverse hydrophobic modification strategies, silanization has been widely adopted for the hydrophobic treatment of nanocellulose owing to its economic efficiency, environmental friendliness and satisfactory modification performance. Meanwhile, silane grafting can generate steric hindrance between CNC particles, further improving the dispersion of CNCs in organic solvents. Common silane reagents for this purpose include hexadecyltrimethoxysilane (HDTMS) [52], methyltrimethoxysilane (MTMS) [34], and methyltrichlorosilane (MTCS) [53], all of which are capable of realizing hydrophobic modification of nanocellulose. As one representative silane candidate, MTMS possesses distinct advantages. Compared with other silane reagents, MTMS features a lower cost and can be readily deposited onto nanocellulose surfaces via a facile and efficient procedure.

In this work, MTMS-silanized cellulose nanocrystals (Si-CNCs) are utilized as multifunctional fillers. It is hypothesized that Si-CNCs can act as superhydrophobic nano building blocks due to their inherent micro/nanoscale morphology, while simultaneously serving as green dispersants for PVDF/PDMS blends. The abundant negative surface charges of Si-CNCs suppress the aggregation of PVDF/PDMS and Si-CNCs through the synergistic effect of steric hindrance, hydrogen bonding and electrostatic repulsion. Superhydrophobic composite microsphere coatings were prepared on cotton fabric, wood board and glass slides via NIPS and ES methods. The regulatory mechanism of Si-CNCs on the surface morphology and wetting performance was systematically explored. Meanwhile, the merits, applicable scenarios and limitations of the NIPS and ES methods were comprehensively compared and discussed. By suppressing PVDF/PDMS aggregation with Si-CNCs, the proposed strategy enables the fabrication of uniformly distributed and structurally stable micro/nanostructures. This work provides technical routes to prepare high-performance superhydrophobic surfaces through a relatively eco-friendly, environmentally sustainable, scalable and substrate-flexible approach, and facilitates high-value applications of CNCs within the industrialization of superhydrophobic materials.

2. Materials and Methods

2.1. Materials

Cellulose microcrystals (CMCs, particle size: ~25 μm) were purchased from Macklin Biochemical Technology Co., Ltd. (Shanghai, China). Polyvinylidene fluoride (PVDF, Mw = 530,000 g/mol), polydimethylsiloxane (PDMS, Sylgard® 184), N,N-dimethylformamide (DMF) and tetrahydrofuran (THF) (AR grade) were obtained from Sigma-Aldrich Trading Co., Ltd. (Shanghai, China). Methyltrimethoxysilane (MTMS) was supplied by Aladdin Biochemical Technology Co., Ltd. (Shanghai, China). Concentrated sulfuric acid (AR grade) was provided by Guangzhou Chemical Reagent Factory (Guangzhou, China).

2.2. Preparation of Cellulose Nanocrystals (CNCs)

Cellulose nanocrystals (CNCs) were successfully prepared from CMCs via sulfuric acid hydrolysis [9]. Briefly, 5 g of CMCs in powder form were uniformly dispersed in 43.6 mL of 64 wt% sulfuric acid under continuous magnetic stirring at 500 rpm (MR Hei-Tec, Heidolph Instruments GmbH & Co. KG, Schwabach, Germany). The mixture was hydrolyzed at 45 °C for 90 min in a water bath with a thermometer, and the reaction was subsequently terminated by adding excessive deionized water. The resulting suspension was dialyzed in dialysis bags with a molecular weight cutoff of 14,000 Da. Dialysis was continued until the conductivity of the external dialysate matched that of pure deionized water, confirming the complete removal of residual chemicals from the suspension. Thereafter, the suspension was centrifuged at 4000 rpm for 15 min (Allegra X-30, Beckman Coulter, Osterode, Germany). After removing the supernatant, deionized water was supplemented for repeated centrifugation cycles until the supernatant presented a faint blue and viscous state. Finally, the viscous supernatant was collected and freeze-dried (FDU-1200, EYELA, Tokyo, Japan) to yield solid CNC powder.

2.3. Preparation of Silanized Cellulose Nanocrystals (Si-CNCs)

The as-prepared CNCs were hydrophobically functionalized with MTMS through a facile vapor deposition strategy with some modifications [54]. Typically, 1 g of as-prepared CNC powder, 210 μL of MTMS, and 630 μL of deionized water were separately placed in Petri dishes and sealed in a closed container. The vapor-phase reaction was conducted at 60 °C for 1 h in an oven. The resulting Si-CNCs were preserved in a desiccator for subsequent experimental use. The reaction mechanism is shown in Figure 1.

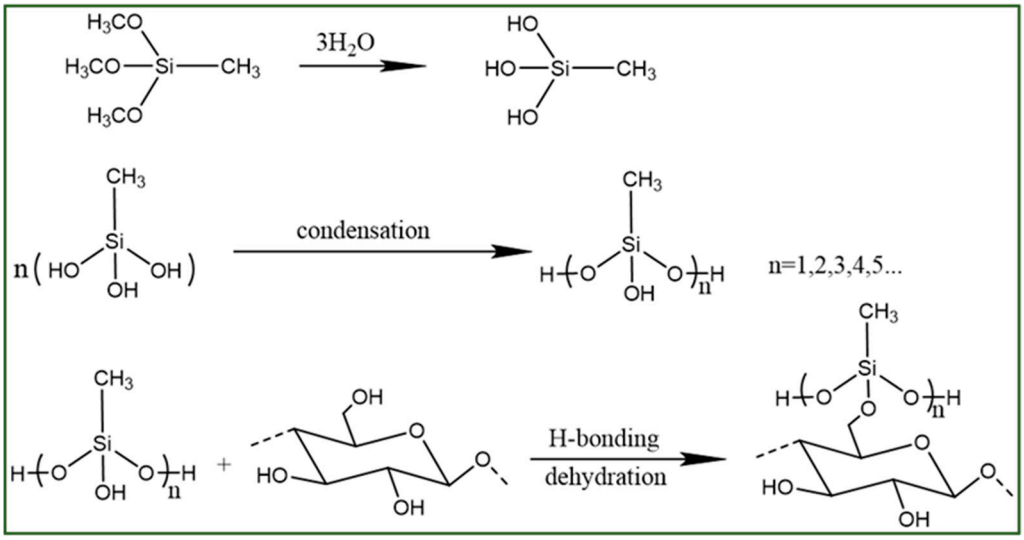


Figure 1. Reaction mechanism diagram of MTMS modification for CNCs.

2.4. Construction of Superhydrophobic Surfaces

2.4.1. Non-Solvent-Induced Phase Separation (NIPS)

First, PDMS (3 wt%) was dissolved in DMF/THF mixed solvent (mass ratio = 1:1). The mixture was magnetically stirred (MR Hei-Tec, Heidolph Instruments GmbH & Co. KG, Schwabach, Germany) at 80 °C in an oil bath for 4 h to achieve complete dissolution. Subsequently, PVDF (2 wt%) was added into the PDMS solution, and the system was stirred continuously at 70 °C for another 4 h to prepare the homogeneous PVDF/PDMS solution. Afterwards, Si-CNCs with mass fractions of 0%, 0.5%, 1%, 1.5% and 2% were introduced individually to achieve 5 different mixed suspensions, which were further ultrasonically treated (JY99-IIDN, Scientz, Ningbo, China) for 1 h to form uniformly dispersed PVDF/PDMS/Si-CNCs suspensions.

Three types of substrates, including cotton fabric (5 cm × 5 cm), wood board (2 cm × 5 cm) and glass slides (2.5 cm × 7.6 cm), were sequentially ultrasonically cleaned (KQ-300DE, Kunshan Ultrasonic Instrument Co., Ltd., Kunshan, China) with anhydrous ethanol and deionized water for three cycles, followed by drying. The pre-treated substrates were soaked in the as-prepared suspensions for 10 min. After removing the residual solution, the samples were immersed in deionized water for 10 min to conduct phase inversion. Finally, all samples were dried in an oven at 50 °C to acquire the target superhydrophobic surfaces. The overall schematic diagram is shown in Figure 2.

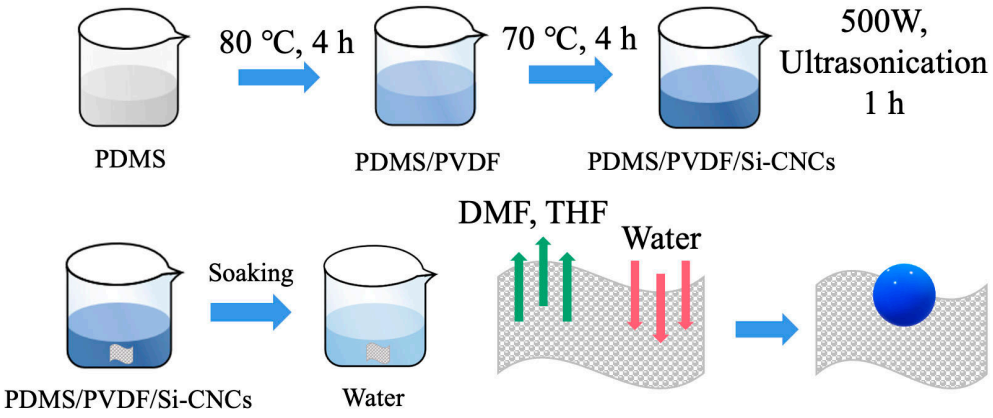


Figure 2. Process diagram of superhydrophobic surface coated by NIPS method.

2.4.2. Electrostatic Spraying (ES)

The PVDF/PDMS solution was prepared following the same procedures described for the NIPS method. Si-CNCs with mass fractions of 0%, 0.5%, 1%, 1.5% and 2% were incorporated, and the mixtures were ultrasonicated (JY99-IIDN, Scientz, Ningbo, China) at 500 W for 1 h to yield homogeneous suspensions. ES was carried out using an SS-2535H device (Yongkang Leye Technology Co., Ltd., Beijing, China) equipped with a 27G needle (inner diameter: 0.19 ± 0.02 mm). The spraying parameters were set as follows: applied voltage of 13 kV, tip-to-collector distance of 8 cm and solution flow rate of 1.5 mL/h. The suspensions were sprayed onto pre-cleaned cotton, wood and glass substrates mounted on the collector. Upon completion, the resultant samples were stored in a desiccator. The overall schematic diagram is shown in Figure 3.

2.5. Characterization

2.5.1. Fourier Transform Infrared Spectroscopy (FT-IR)

Freeze-dried CMC, CNC, and Si-CNC powders (5 mg) were homogeneously blended with KBr powder and pressed into pellets, respectively. The chemical functional groups

of the samples were characterized using an FT-IR spectrometer (Vertex 70, Bruker Optics, Ettlingen, Germany) within the wavenumber range of 400–4000 cm^{-1}.

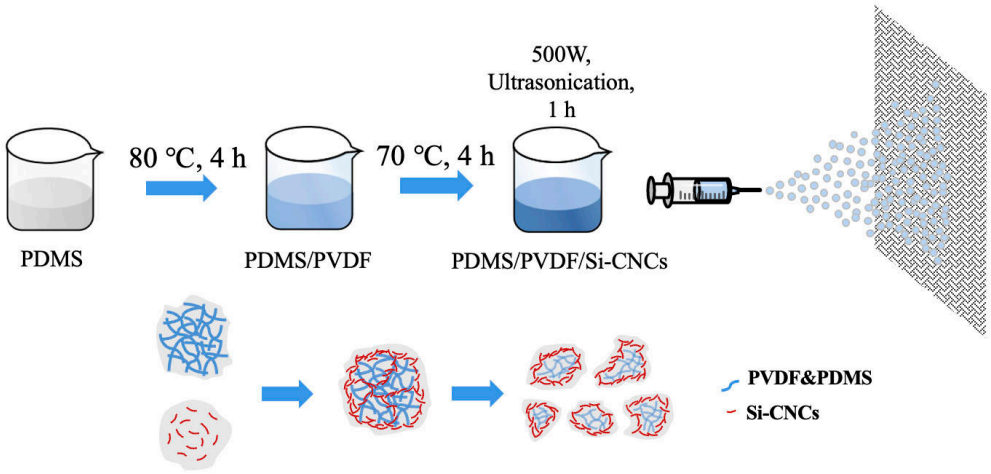


Figure 3. Process diagram of superhydrophobic surface coated by ES method.

2.5.2. X-Ray Photoelectron Spectroscopy (XPS)

The surface elemental composition and chemical bonding states of the samples were analyzed via XPS (K-Alpha, ThermoFisher Scientific Inc., Waltham, MA, USA) equipped with monochromatic Al Kα radiation (150 W). The pass energy was set to 160 eV for survey spectra and 40 eV for high-resolution spectra, and the test chamber vacuum was maintained below 5×10^{-9} Torr.

2.5.3. Atomic Force Microscopy (AFM)

The aqueous suspensions of CNCs and Si-CNCs were diluted to approximately 0.1‰ and uniformly dispersed by ultrasonication (JY99-IIDN, Scientz, Ningbo, China). The diluted suspensions were drop-cast onto freshly cleaned mica substrates and dried naturally. The microscopic morphology and surface topography of the samples were characterized by AFM (Multimode 8, Bruker Corporation, Santa Barbara, CA, USA).

2.5.4. Scanning Electron Microscopy (SEM)

The surface microstructures of the raw and modified cotton fabric were observed using a field emission scanning electron microscope (Merlin, Carl Zeiss, Oberkochen, Germany). Prior to observation, all samples were sputter-coated with a thin gold layer to enhance surface conductivity, and imaging was performed at different magnifications.

2.5.5. Water Contact Angle (WCA) and Sliding Angle (SA) Measurements

The static WCA and SA of the superhydrophobic surfaces were measured using a micro contact angle measuring instrument (OCA40, Dataphysics, Filderstadt, Germany) with a 5 µL deionized water droplet. For each sample, five random positions were tested to obtain the average value. In addition, the time-dependent variations in WCA at 2.5 min and 5 min were continuously recorded.

2.5.6. Abrasion Resistance Test

The mechanical abrasion resistance of the superhydrophobic surfaces was evaluated using 320-grit sandpaper under a constant pressure of 35 kPa (350 g load) [55]. The modified surfaces of the three substrates were subjected to unidirectional reciprocating friction from left to right with a fixed stroke length of 10 cm. The sandpaper was replaced after testing each sample. After different abrasion cycles, the WCA and SA variations in the surfaces

were measured with a micro contact angle measuring instrument (OCA40, Dataphysics, Filderstadt, Germany). Furthermore, the surface morphological changes in the samples after abrasion were observed by SEM (Merlin, Carl Zeiss, Oberkochen, Germany).

3. Results and Discussion

3.1. Chemical Structure and Morphology of Cellulose Samples

3.1.1. FTIR and AFM of CNCs

FTIR characterization was performed on CMC and CNC samples to evaluate the final effect of sulfuric acid hydrolysis of CMCs. As shown on Figure 4a, the peaks at 1060 cm^{-1} and 3431 cm^{-1} correspond to the C-O-C stretching vibration of the pyranose ring and the free O-H single-bond stretching vibration of hydroxyl groups in cellulose, respectively. The absorption bands at 2903 cm^{-1} and 1430 cm^{-1} arise from C-H stretching and bending of CH_2 groups [56]. These results clearly reveal the typical structural characteristics of cellulose and are consistent with CNCs extracted from other feedstocks. Compared with the FTIR spectrum of CMCs, a new absorption peak appears at 805 cm^{-1} for CNCs, which is assigned to the symmetric C-O-S vibration of the C-O-SO_3^- group [57]. This confirms that sulfate groups were successfully introduced onto the surfaces of CNCs.

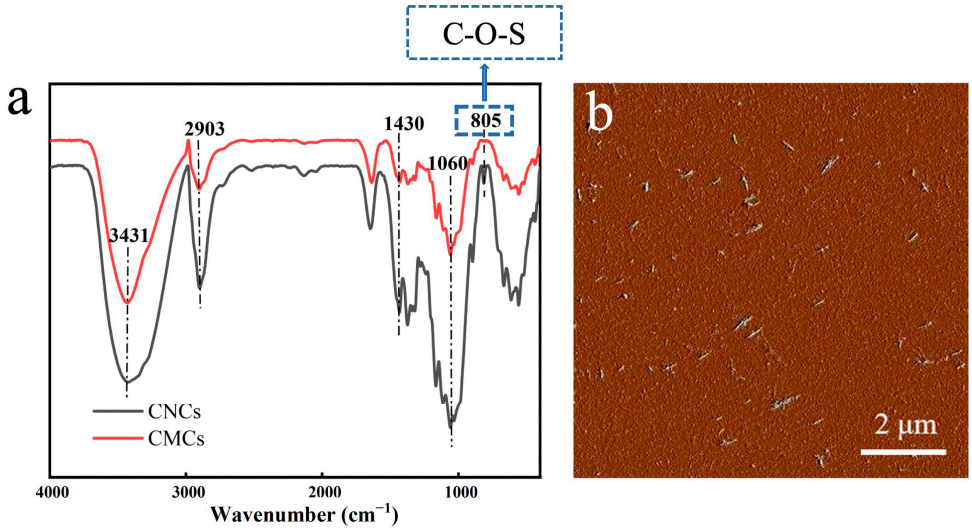


Figure 4. (**a**) FTIR spectra of CNCs and CMCs; (**b**) AFM images of CNCs.

As observed in the AFM image (Figure 4b), the CNCs display a short rod-like structure with a good dispersion. During sulfuric acid hydrolysis, anionic sulfate ester groups are grafted onto the surface hydroxyl groups of cellulose. These negatively charged moieties effectively facilitate the dispersion of CNCs in water through electrostatic repulsion, thereby contributing to the improvement of material properties [58]. Statistical analysis of more than 100 CNCs was carried out using image analysis software. The average diameter was determined to be 14 ± 5 nm, with the length ranging from 56 nm to 278 nm. The formation of superhydrophobic surfaces generally originates from the accumulation of nanoparticles or hybrid micro/nano-sized particles. Shorter nanofibers are more favorable for constructing finer, more uniform and stable rough structures on the particle surfaces [25].

3.1.2. FTIR, XPS and AFM of Si-CNCs

Figure 5a displays the FTIR spectra of pristine CNCs and silane-modified Si-CNCs. As observed, Si-CNCs still retain the typical characteristic peaks of cellulose, indicating that the fundamental structure of CNCs is not altered after modification [31]. Compared with unmodified CNCs, a new absorption band appears at 1270 cm^{-1} in the spectrum of

Si-CNCs, which is assigned to the C-H bending vibration of Si-CH_3 groups from MTMS, confirming the presence of silane moieties [52,53,59,60]. Meanwhile, the strong absorption peak at 766 cm^{-1} corresponds to the symmetric stretching vibration of Si-C or Si-O-Si bonds formed during silanization [52,59], further confirming the successful silane modification of CNCs. Moreover, as reported in related silanization research, characteristic signals of Si-OCH_3 and Si-C bonds can also be observed at higher wavenumbers of approximately 1092 cm^{-1} and 1190 cm^{-1} [61], but they were not observed clearly in this study, probably because they were overlapped by the large and intense cellulose C–O stretching band in cellulose [52,62,63].

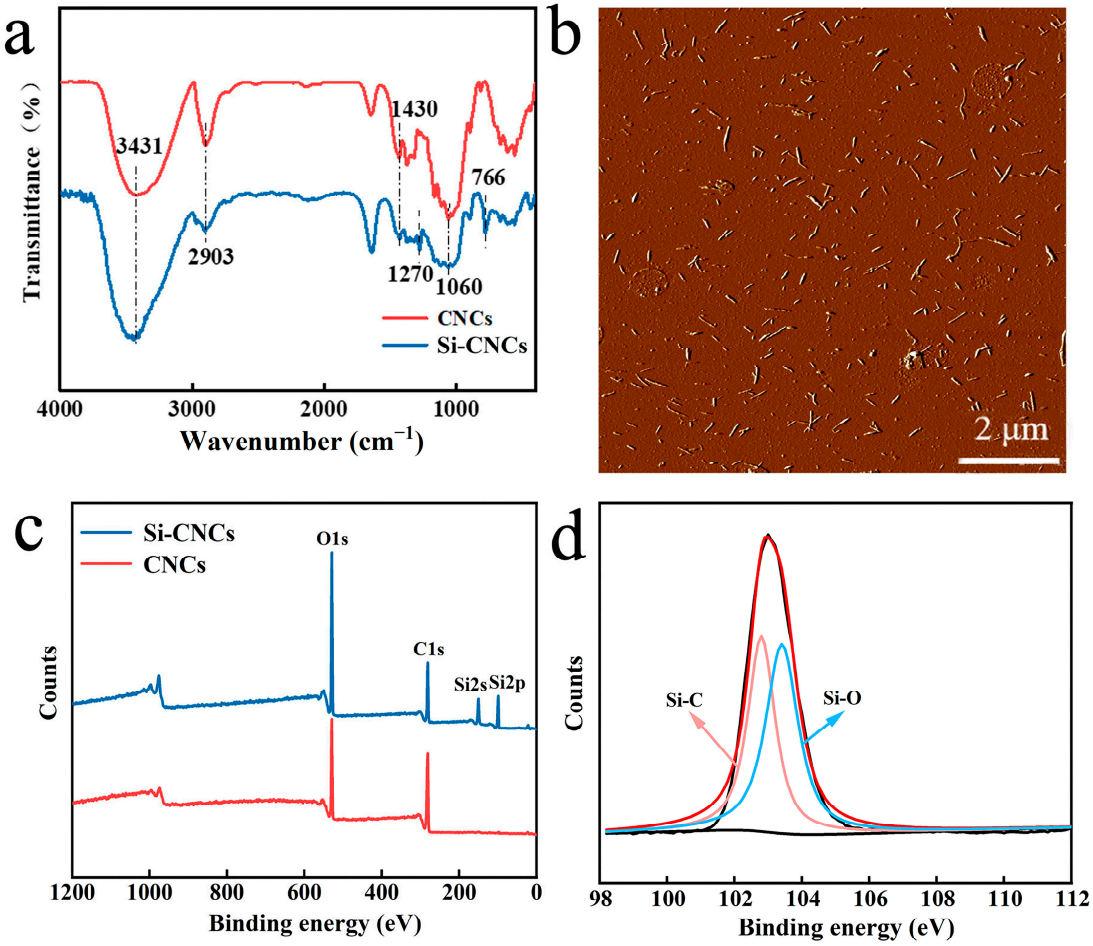


Figure 5. (**a**) FT-IR images of CNCs and Si-CNCs; (**b**) AFM image of Si-CNCs; (**c**) full spectrum of XPS images of CNCs and Si-CNCs; (**d**) high-resolution spectrum of Si2p of Si-CNCs.

AFM characterization was further conducted to investigate the morphological features of Si-CNCs. The results (Figure 5b) reveal that the modification exerts negligible effects on the morphology and size of CNCs. The as-prepared Si-CNCs maintain a short rod-like morphology with a favorable dispersion state. Statistical analysis shows that the average diameter of Si-CNCs is 13 ± 6 nm, while their lengths range from 38 nm to 249 nm.

XPS measurements were performed to further explore the chemical variations in CNCs before and after modification. As presented in Figure 5c,d, only carbon and oxygen signals are detected for pristine CNCs. In contrast, two new characteristic peaks assigned to Si2p and Si2s emerge on the surface of modified Si-CNCs, demonstrating the presence of the silicon element. Figure 5d shows the high-resolution XPS spectrum of Si2p for Si-CNCs after peak fitting. Two distinct peaks located at 102.1 eV and 103.62 eV are attributed to Si-C and Si-O bonds, respectively [64]. During the silanization process, the Si-OCH_3 groups

of MTMS are readily hydrolyzed into unstable Si-OH groups, which subsequently undergo condensation reactions. A portion of silanol groups self-polymerizes to form oligomers. The residual Si-OH groups and silanol oligomers interact with the free hydroxyl groups on the CNC surface via dehydration condensation, when Si-OH loses hydroxyl groups and CNC hydroxyl groups lose hydrogen atoms, thereby covalently grafting MTMS onto CNCs [64]. To summarize from above, the XPS results further verify the successful silane modification of CNCs with MTMS.

3.2. Effect of Si-CNCs on Morphological Modification of Cotton Fabric Surface

3.2.1. NIPS-Prepared Surfaces

Cotton fabrics were treated with PVDF/PDMS/Si-CNC mixed solution via the NIPS method. Figure 6 presents the surface morphology of cotton fabrics before and after treatment with different Si-CNC additions. Figure 6a_1,a_2 shows SEM images of pristine cotton fabric without hydrophobic treatment at two different magnifications. Figure 6b_1–f_2 display the surface morphologies of cotton fabrics modified by mixed solutions with Si-CNC mass fractions of 0%, 0.5%, 1%, 1.5% and 2%, respectively, at various magnifications.

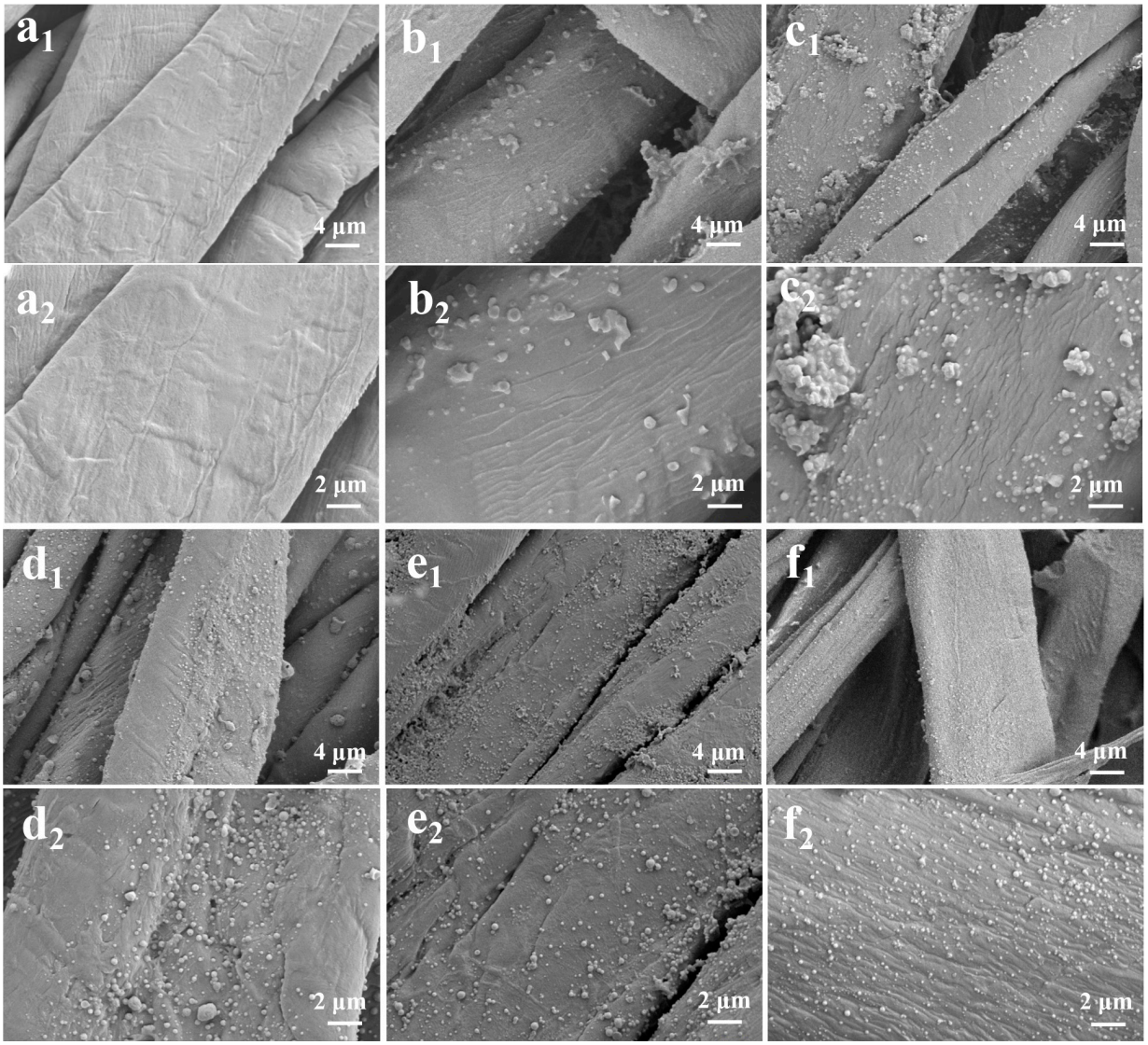


Figure 6. SEM images of (**a_1**,**a_2**) pristine cotton fabric fibers without superhydrophobic coating, and coated cotton fabric fibers fabricated via the NIPS method using PVDF/PDMS suspensions loaded with (**b_1**,**b_2**) 0%, (**c_1**,**c_2**) 0.5%, (**d_1**,**d_2**) 1%, (**e_1**,**e_2**) 1.5% and (**f_1**,**f_2**) 2% Si-CNCs.

SEM observations indicate that when Si-CNCs were absent (Figure 6b_1,b_2) or added at a low loading (Figure 6c_1,c_2), the cotton fabric surface was covered by heavily agglomerated polymers with large and unevenly dispersed particles. With the increase in Si-CNC mass fraction (Figure 6d_1–f_2), particle agglomeration on the fabric surface was remarkably alleviated, and a uniform rough structure with well-distributed particles was gradually formed. This trend is consistent with our previous work using unmodified CNCs to construct hydrophobic coatings on cotton fabrics [25]. Notably, the particles on fabrics treated with Si-CNCs exhibited a distinctly smaller size. This can be explained by the grafted MTMS chains on the CNC surface, as MTMS reduces the surface energy of CNCs. Meanwhile, the overlapping grafted polymer layers generate steric hindrance between Si-CNCs, which further improves their dispersibility. During NIPS, Si-CNCs co-agglomerate with PVDF and PDMS. The combined effects of electrostatic repulsion and steric hindrance among exposed Si-CNCs inhibit excessive particle growth and effectively enhance the dispersion of the formed particles [25].

3.2.2. ES-Prepared Surfaces

The mixed solutions containing different mass fractions of Si-CNCs were sprayed onto cotton fabrics via electrostatic spraying. Figure 7 shows the surface morphology of cotton fabrics sprayed with Si-CNCs at varying mass fractions under different magnifications.

As illustrated in SEM images, consistent with the enhancement effect of the NIPS method, the cotton fabric surface was covered with severely agglomerated polymers with large-sized and unevenly dispersed particles in the absence of Si-CNCs (Figure 7b_1,b_2) or at a low Si-CNC dosage (Figure 7c_1,c_2). When the mass fraction of Si-CNCs increased above 1%, the particle dispersibility was greatly improved, and the size of microspheres on the cotton fabric surface decreased significantly. As presented in Figure 8, the particle size of ES coatings gradually decreases from several micrometers to the nanometer scale with an increasing Si-CNC content, revealing the enhanced dispersing effect of Si-CNCs on the PVDF/PDMS system during the ES coating process. In the electrostatic spraying process, the charge density serves as a critical factor affecting the microsphere morphology of sprayed coatings. The surface charge of Si-CNCs remains unchanged, and the electrostatic field force dominates the spraying process. Therefore, the steric hindrance induced by silane modification exerts a negligible effect on the overall surface morphology.

In summary, Si-CNCs can effectively disperse polymer aggregates on cotton fabric surfaces fabricated by both the NIPS and ES methods. The low-surface-energy polymer particles on the modified cotton fabrics possess a smaller particle size and uniform distribution, which is beneficial to the improvement of the superhydrophobic performance of cotton fabrics. Nevertheless, the morphological differences between the two fabrication methods are difficult to distinguish merely by SEM observation. At identical Si-CNC loadings, surface particles on cotton fabric coated via the NIPS method are evidently finer than those obtained by the ES method. To further verify the practical modification effect of Si-CNCs on the superhydrophobic properties of substrates via the two methods, superhydrophobic coatings were constructed on wood and glass substrates through the above two strategies. The wettability and friction resistance of the modified cotton fabric, wood and glass surfaces were systematically tested and compared.

3.3. Wettability Performance

3.3.1. NIPS-Prepared Surfaces

Mixed solutions with different mass fractions of Si-CNCs were employed to treat three substrates (cotton fabric, wood and glass) via the NIPS method. Deionized water droplets of 5 μm were deposited on the substrate surfaces to measure the water contact angle (WCA)

and sliding angle (SA). Meanwhile, the variation in WCA within 5 min was continuously monitored and recorded (Figure 9).

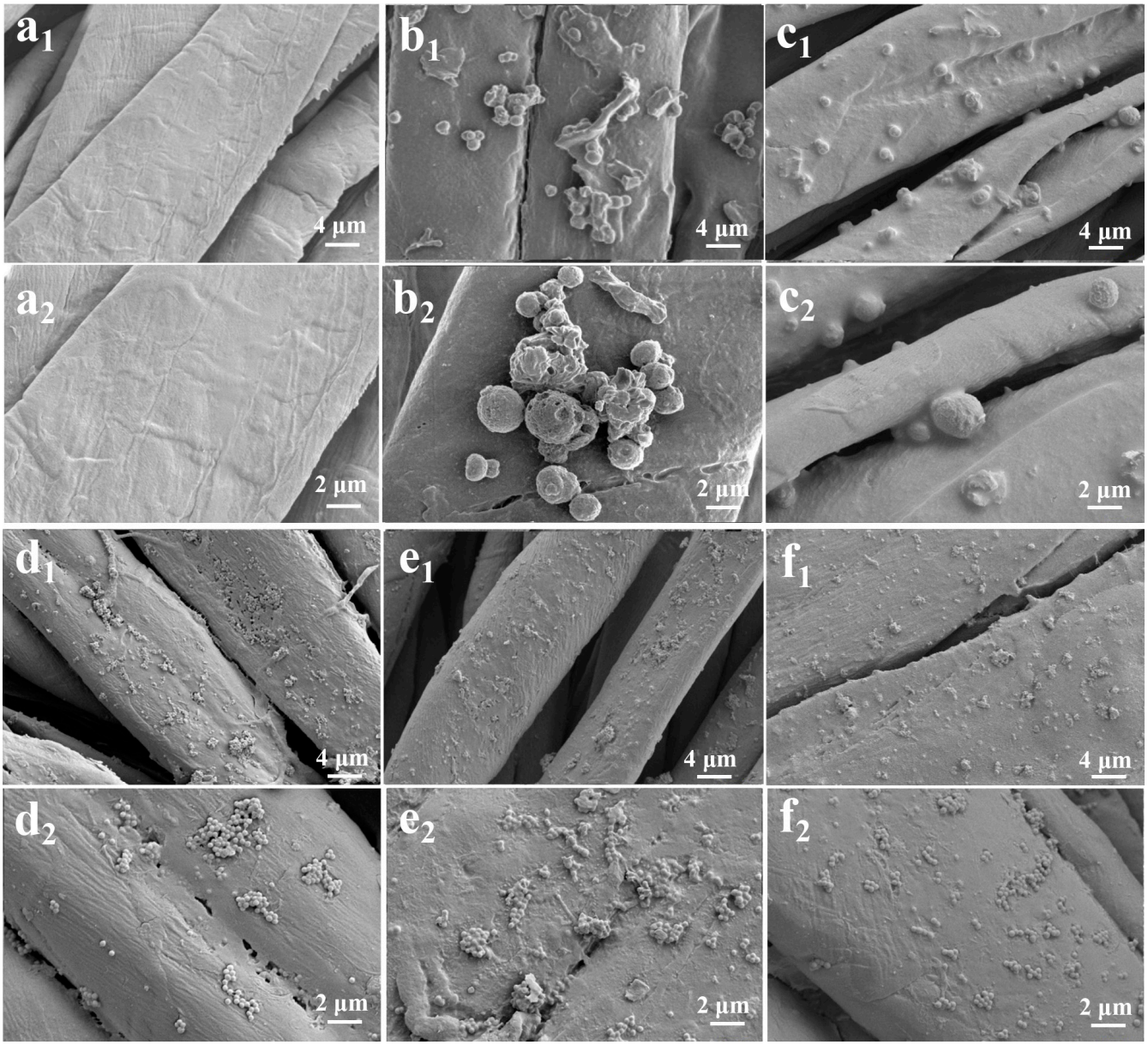


Figure 7. SEM images of (**a**$_1$,**a**$_2$) pristine cotton fabric fibers without superhydrophobic coating, and coated cotton fabric fibers fabricated via the ES method using PVDF/PDMS suspensions loaded with (**b**$_1$,**b**$_2$) 0%, (**c**$_1$,**c**$_2$) 0.5%, (**d**$_1$,**d**$_2$) 1%, (**e**$_1$,**e**$_2$) 1.5% and (**f**$_1$,**f**$_2$) 2% Si-CNCs.

As displayed in Figure 9a, with the increase in Si-CNC loading, the WCA of the modified cotton fabric increased first and then decreased, with corresponding values of 143°, 149°, 152° 156° and 151°, and the minimum SA was 3.5°. Combined with the particle distribution morphology of cotton fabric analyzed above (Figure 6), during the increase in Si-CNC mass fraction up to 1.5%, the dispersion uniformity of surface particles was gradually improved, while the particle size became more uniform and decreased progressively. Although slight particle aggregation still existed, the surface successfully formed a well-dispersed micro/nano hierarchical rough structure. Furthermore, Figure 9b,c illustrates the variations in WCA and SA of water droplets on modified wood and glass substrates, respectively. Similarly, the WCA for wood and glass surfaces increased first and then decreased with the elevation in Si-CNC loading, exhibiting the same variation

trend as cotton fabric. Due to the inherent differences in substrate properties, the modified wood and glass surfaces presented a lower WCA and slightly inferior superhydrophobicity compared with cotton fabric.

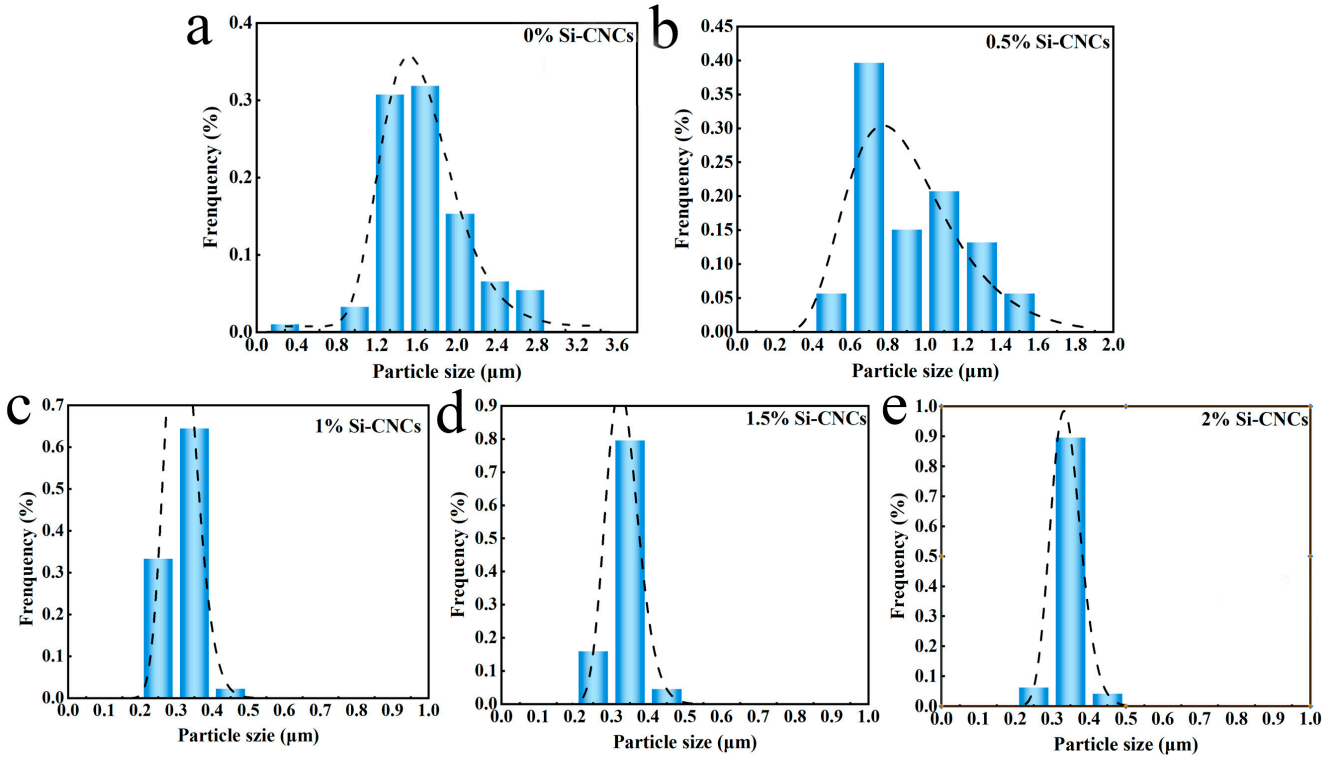


Figure 8. Particle size distribution on the cotton fabric fiber surfaces coated via the ES method using PVDF/PDMS suspensions loaded with (**a**) 0%, (**b**) 0.5%, (**c**) 1%, (**d**) 1.5% and (**e**) 2% Si-CNCs.

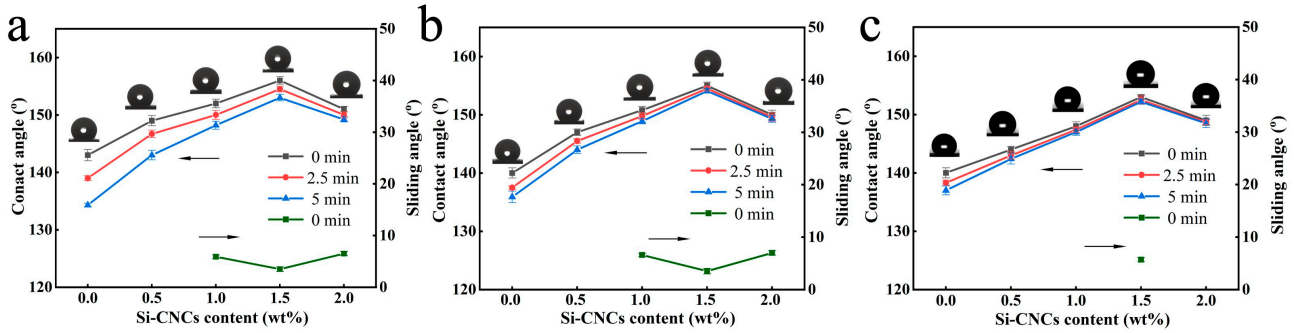


Figure 9. Evolution of WCA and SA of water drops on the surface of (**a**) cotton fabric, (**b**) wood and (**c**) glass after hydrophobic coating treatment by NIPS method.

Furthermore, the superhydrophobic performance of substrates modified with Si-CNCs was compared with that of substrates modified with pristine CNCs [25]. At Si-CNC mass fractions of no more than 1.5%, the substrates modified with Si-CNCs exhibited slightly lower WCAs than those modified with unmodified CNCs. The reason is that although Si-CNCs effectively inhibited polymer aggregation and reduced the particle size, the excessively fine particles decreased the surface roughness. However, the silane modification endowed CNCs with intrinsic hydrophobicity, which further reduced the surface free energy of the modified substrates. The synergistic effect of reduced roughness and low surface energy resulted in negligible differences in the overall WCA and SA before and after modification. Notably, the superhydrophobic surfaces modified with Si-CNCs exhibited smaller WCA attenuation over time and improved long-term stability compared

with the pristine CNCs-modified surfaces [25]. This phenomenon indicates that a reduced particle size and enhanced particle dispersion are beneficial to improving the temporal stability of the contact angle of superhydrophobic surfaces.

3.3.2. ES-Prepared Surfaces

The superhydrophobic surfaces fabricated via the ES method followed a similar variation trend but achieved enhanced hydrophobicity compared with those prepared by the NIPS method, and the optimal performance was also obtained at the Si-CNC mass fraction of 1.5%. As shown in Figure 10, the WCA value for cotton fabric, wood and glass surfaces continuously increased with the elevation of Si-CNC loading, reaching maximum values of 168.7°, 165.8° and 161°, respectively. Compared with the maximum WCA of coatings fabricated by the NIPS method on the corresponding substrates, the values of ES coatings increased by approximately 12°, 10° and 9° for cotton fabric, wood and glass, respectively. Meanwhile, the SA decreased gradually to minimum values of 0.8°, 1.0° and 1.7°, which were significantly lower than the minimum SA of about 3.5° obtained from the NIPS method.

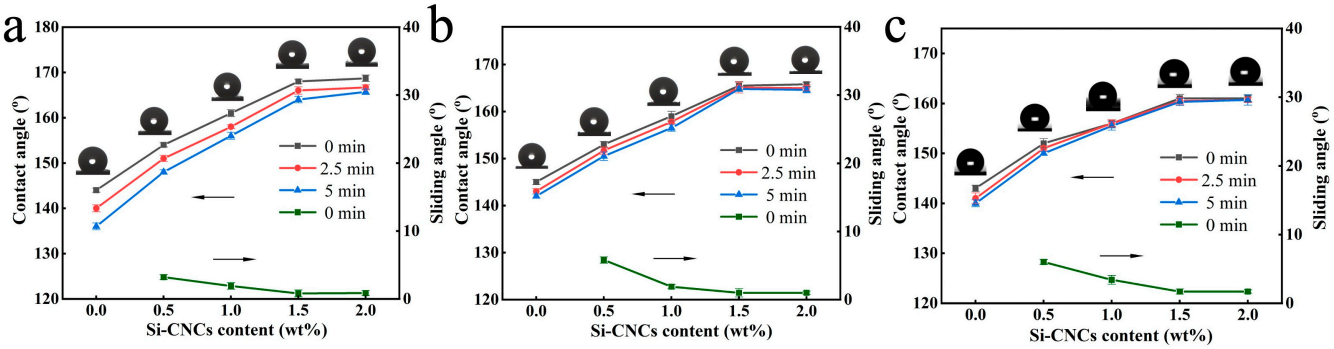


Figure 10. Evolution of WCA and SA of water drops on the surface of (**a**) cotton fabric, (**b**) wood and (**c**) glass after hydrophobic coating treatment by ES method.

This difference and tendency can be rationalized by considering that with increasing Si-CNC loading, surface particles are refined to nanoscale dimensions (Figure 8), which hinders the construction of required micro/nanoscale hierarchical roughness and thus reduces the WCA. Combined with the consistent morphological evolution of NIPS and ES coatings observed from SEM micrographs (Figures 6 and 7), and the quantitative particle size distribution trend of ES samples (Figure 8), we deduce that the particle size of NIPS coatings probably also declines progressively with elevated Si-CNC loading and remains smaller than that of ES counterparts under identical preparation conditions. This structural evolution explains the degraded wettability observed at 2% Si-CNC loading for both coating methods. Excess Si-CNCs further refine surface particles and greatly suppress the formation of microscale aggregates, which prevents the generation of fully developed micro/nanoscale hierarchical roughness. The absence of multiscale roughness ultimately results in a lower WCA and larger SA, leading to a deteriorated superhydrophobic performance.

In addition, the time-dependent attenuation of the WCA was further weakened, demonstrating improved long-term stability of the ES superhydrophobic surfaces. Such performance enhancement is probably attributed to the intrinsic hydrophobicity of Si-CNCs. During electrostatic spraying, partial Si-CNCs are exposed on the surface of polymer microspheres, which further reduces the overall surface free energy of the substrates and ultimately improves the superhydrophobic performance of the coatings.

3.4. Mechanical Abrasion Resistance

3.4.1. NIPS-Prepared Surfaces

Superhydrophobic coatings were fabricated on cotton fabric, wood and glass substrates via the NIPS method using the mixed solution with 1.5% Si-CNCs. The mechanical friction resistance of the coatings was evaluated, and the variations in surface WCA and SA after different friction cycles were systematically investigated. As shown in Figure 11, the changing trends of WCA and SA with increasing friction cycles for the Si-CNC-modified coatings on three substrates were essentially consistent with those of pristine CNC-based superhydrophobic surfaces prepared via NIPS [25]. Nevertheless, after silane modification, the cotton fabric (Figure 11a) and wood surfaces (Figure 11b) maintained a WCA value above 150° within 820 friction cycles and retained stable superhydrophobicity. However, after 800 friction cycles (Figure 11d,e) for the cotton fabric specimens, the micro/nano hierarchical rough structure was compromised, which significantly reduced the superhydrophobic performance of the modified cotton fabric surface, although a substantial number of uniformly dispersed microspheres remained on the surface. In contrast, the modified glass substrate could sustain its superhydrophobic performance within 400 friction cycles (Figure 11c).

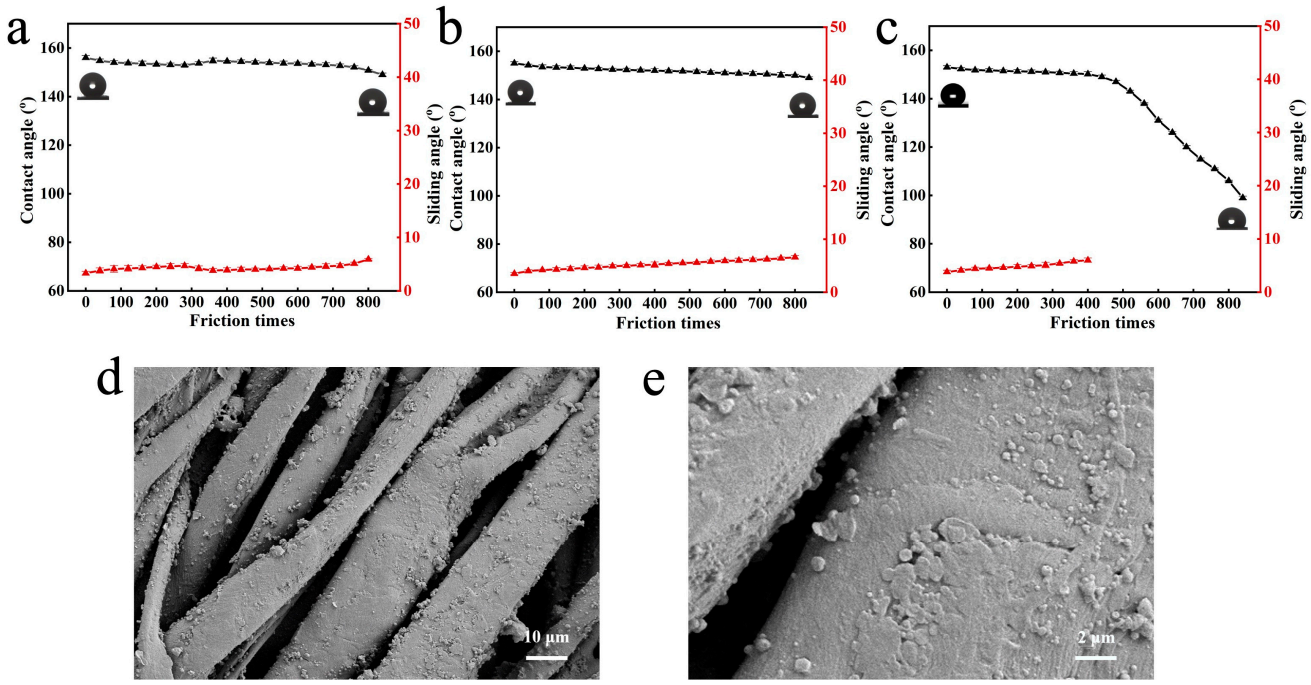


Figure 11. Evolution of superhydrophobic abrasion resistance for NIPS-coated (**a**) cotton fabric, (**b**) wood and (**c**) glass substrates with 1.5% Si-CNC loading; (**d**,**e**) SEM images of 1.5% Si-CNC-modified cotton fabric fibers after 800 abrasion cycles.

Overall, the Si-CNC-modified superhydrophobic surfaces exhibited significantly improved friction resistance compared with the pristine CNC-modified coatings. This improvement is mainly attributed to the optimized microstructure induced by Si-CNCs. The incorporation of Si-CNCs effectively inhibited polymer aggregation during the NIPS process and reduced the particle size of the coating. The refined particles increased the contact area between the coating and the substrate, thereby enhancing the interfacial adhesion strength. The improved adhesion enabled the coating to withstand more cycles of mechanical friction and maintain a stable superhydrophobic performance.

3.4.2. ES-Prepared Surfaces

Similar to the NIPS method, superhydrophobic surfaces were fabricated on three substrates via the ES method using a mixed solution containing 1.5% Si-CNCs, and the resulting coatings also possessed excellent friction resistance. As shown in Figure 12, the coated cotton fabric and wood maintained WCAs above 150° and SAs below 8° within 550 friction cycles, while the coated glass retained stable superhydrophobicity within 470 friction cycles. However, the friction resistance of ES superhydrophobic surfaces was relatively inferior to that of the coatings prepared by the NIPS method. This difference originates from the distinct formation mechanisms of the two coating strategies. The ES method relies mainly on physical stacking to construct surface structures, producing loose and single-level micro/nano-architectures, in which Si-CNCs tend to exist as isolated particles or aggregates. Meanwhile, both the interfacial bonding between the coating and the substrate and the internal cohesion of the coating are weak. In contrast, the NIPS method enables the self-assembly of polymers to form a continuous and interpenetrating porous network structure, in which Si-CNCs are firmly anchored. This structure significantly enhances the internal cohesion and interfacial adhesion of the coating, thereby guaranteeing superior surface structural stability. As shown in Figure 12d,e, after 550 friction cycles, a large number of microspheres had detached from the cotton fabric surface, and fewer microspheres remained on the substrate compared to those on the NIPS-coated cotton fabrics even after 800 friction cycles.

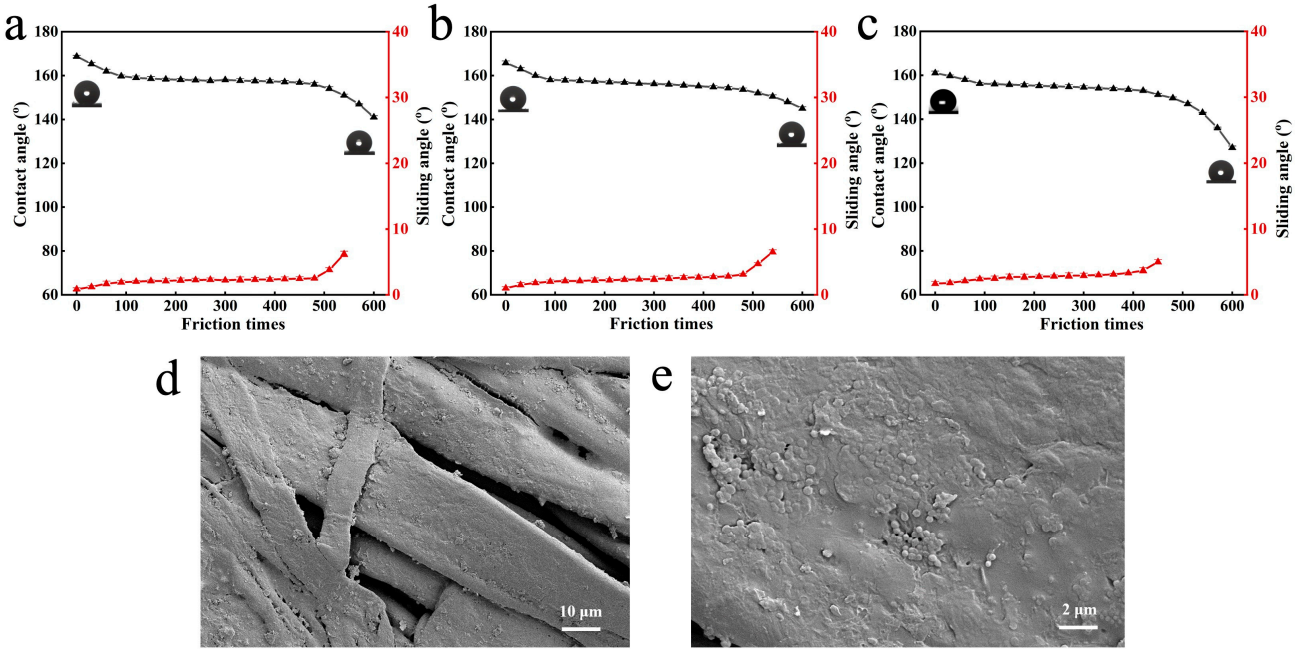


Figure 12. Evolution of superhydrophobic abrasion resistance for ES-coated (**a**) cotton fabric, (**b**) wood and (**c**) glass substrates with 1.5% Si-CNC loading; (**d**,**e**) SEM images of 1.5% Si-CNC-modified cotton fabric fibers after 550 abrasion cycles.

Overall, the superhydrophobic surfaces fabricated by the two strategies based on Si-CNCs exhibited outstanding friction durability. On the one hand, PDMS is a flexible elastic polymer that can achieve structural recovery after the removal of external force, endowing the composite coating with excellent wear resistance [65]. On the other hand, PDMS possesses a superior adhesive performance, which effectively strengthens the interfacial bonding force between micro/nanoparticles and the substrate. In addition, cotton fabric and wood inherently present natural rough surface morphologies. Partial Si-CNC particles can be embedded in the depressions and grooves of the substrate surface, avoiding direct

shear damage from external forces during friction, which allows the coating to maintain stable superhydrophobic properties after multiple friction cycles.

Notably, pristine cotton fabric and wood are hydrophilic substrates. After modification in this work, the uniformity of the microscopic rough structures on the two substrates was greatly improved, and the surface wettability was efficiently converted from hydrophilicity to superhydrophobicity. These results fully confirm that Si-CNCs can be uniformly dispersed in the PVDF/PDMS composite system and play a critical regulatory role in constructing stable rough interfaces and synergistically enhancing the superhydrophobic performance of substrates.

4. Conclusions

In this work, methyltrimethoxysilane-modified cellulose nanocrystals (Si-CNCs) were adopted as high-efficiency reinforcing functional fillers for superhydrophobic coatings. Combined with low-surface-energy polymers PVDF and PDMS, micro/nanocomposite rough structures were successfully constructed on the surfaces of three typical substrates (cotton fabric, wood and glass) via NIPS and ES approaches to obtain high-performance superhydrophobic composite coatings. Si-CNCs play an efficient dual role in tuning the microstructure and hydrophobic behavior of coatings from both preparation routes. On the one hand, Si-CNCs serve as eco- and environmentally friendly nano building blocks relying on their intrinsic nanostructure to create micro/nanoscale hierarchical roughness on substrate surfaces. On the other hand, driven by synergistic electrostatic repulsion and steric hindrance, Si-CNCs suppress severe aggregation of PVDF/PDMS blends, improve particle dispersion homogeneity and refine the particle size, thus optimizing the microscale roughness of coatings. Significant differences in hydrophobic performance are observed between the two preparation processes. ES-derived coatings display superior superhydrophobicity, with WCAs of 160–166° and a minimum SA of 1°. By contrast, NIPS coatings achieve WCAs of 153.8–158° and SAs of around 2°. In addition, coatings from both methods feature favorable mechanical abrasion stability. For NIPS samples, cotton fabric and wood maintain WCAs > 150° after 820 abrasion cycles, whereas glass sustains stable superhydrophobicity after 400 cycles. For ES samples, cotton fabric and wood retain superhydrophobicity within 550 cycles, and glass maintains WCAs above 150° within 470 cycles. Overall, NIPS coatings exhibit better abrasion resistance and structural stability.

We would like to clarify that the primary objective of this work is to verify the feasibility of using renewable cellulose-based nanomaterials (Si-CNCs) to enhance the performance of PVDF/PDMS superhydrophobic coatings, aiming to establish a facile, scalable, relatively eco-friendly, environmentally sustainable and industry-compatible strategy to alleviate PVDF/PDMS aggregation and fabricate durable superhydrophobic coatings. This study is not designed for comprehensive fundamental characterization of the Si-CNC modification mechanism. Systematic quantitative measurements, including those of the particle size distribution, grafting density of Si-, ζ-potential, surface roughness, etc., will be carried out in further fundamental investigations to deeply reveal the underlying mechanisms. Solvent recovery strategies for DMF and THF, together with the coating's resistance to various environmental conditions, should also be taken into account to further boost the economic and environmental merits of practical industrial deployment.

Author Contributions: Conceptualization, T.S.; methodology, T.S.; formal analysis, J.J.; investigation, J.J.; resources, T.S.; writing—original draft preparation, J.J.; writing—review and editing, T.S., T.H. and A.D.; visualization, J.J.; supervision, T.S.; funding acquisition, T.S. and A.D. All authors have read and agreed to the published version of the manuscript.

Funding: This research was funded by the National Natural Science Foundation of China (22578140) and the Project to Attract Foreign Experts by MOST (H20250222). LGP2 is part of the LabEx Tec 21 (Investissements d'Avenir; Grant Agreement ANR-11-LABX-0030) and PolyNat Carnot Institute (Investissements d'Avenir; Grant Agreement ANR-11-CARN-030-01).

Institutional Review Board Statement: Not applicable.

Data Availability Statement: The raw data supporting the conclusions of this article will be made available by the authors on request.

Conflicts of Interest: The authors declare no conflicts of interest.

Abbreviations

The following abbreviations are used in this manuscript:

PVDF	Polyvinylidene fluoride
PDMS	Poly(dimethylsiloxane)
CMCs	Cellulose microcrystals
CNCs	Cellulose nanocrystals
Si-CNCs	Methyltrimethoxysilane-modified cellulose nanocrystals
NIPS	Non-solvent-induced phase separation
ES	Electrostatic spraying
WCA	Water contact angle
SA	Sliding angle

References

1. Autumn, K.; Gravish, N. Gecko adhesion: Evolutionary nanotechnology. *Philos. Trans. R. Soc. A* **2008**, *366*, 1575–1590. [CrossRef] [PubMed]
2. Ganesh, V.A.; Raut, H.K.; Nair, A.S.; Ramakrishna, S. A review on self-cleaning coatings. *J. Mater. Chem.* **2011**, *21*, 16304–16322. [CrossRef]
3. Liu, K.; Huang, Z.; Hemmatifar, A.; Oyarzun, D.I.; Zhou, J.; Santiago, J.G. Self-Cleaning Porous Surfaces for Dry Condensation. *ACS Appl. Mater. Interfaces* **2018**, *10*, 26759–26764. [CrossRef] [PubMed]
4. Bake, A.; Merah, N.; Matin, A.; Gondal, M.; Qahtan, T.; Abu-Dheir, N. Preparation of transparent and robust superhydrophobic surfaces for self-cleaning applications. *Prog. Org. Coat.* **2018**, *122*, 170–179. [CrossRef]
5. Liu, K.; Zhang, M.; Zhai, J. Bioinspired construction of Mg–Li alloys surfaces with stable superhydrophobicity and improved corrosion resistance. *Appl. Phys. Lett.* **2008**, *92*, 183106. [CrossRef]
6. Xiang, T.; Ding, S.; Li, C.; Zheng, S.; Hu, W.; Wang, J.; Liu, P. Effect of current density on wettability and corrosion resistance of superhydrophobic nickel coating deposited on low carbon steel. *Mater. Des.* **2017**, *114*, 65–72. [CrossRef]
7. Lv, J.; Song, Y.; Jiang, L. Bio-inspired strategies for anti-icing. *ACS Nano* **2014**, *8*, 3152–3169. [CrossRef] [PubMed]
8. Lin, Y.; Chen, H.; Wang, G.; Liu, A. Recent Progress in Preparation and Anti-Icing Applications of Superhydrophobic Coatings. *Coatings* **2018**, *8*, 208. [CrossRef]
9. Wang, N.; Tang, L.; Tong, W.; Xiong, D. Fabrication of robust and scalable superhydrophobic surfaces and investigation of their anti-icing properties. *Mater. Des.* **2018**, *156*, 320–328. [CrossRef]
10. Rajiv, S.; Kumaran, S.; Sathish, M. Long-term-durable anti-icing superhydrophobic composite coatings. *J. Appl. Polym. Sci.* **2018**, *136*, 47059. [CrossRef]
11. Gao, X.; Zhou, J.; Du, R.; Xie, Z.; Deng, S.; Liu, R.; Liu, Z.; Zhang, J. Robust Superhydrophobic Foam: A Graphdiyne-Based Hierarchical Architecture for Oil/Water Separation. *Adv. Mater.* **2016**, *28*, 168–173. [CrossRef] [PubMed]
12. Zhu, H.; Chen, D.; An, W.; Li, N.; Xu, Q.; Li, H.; He, J.; Lu, J. A Robust and Cost-Effective Superhydrophobic Graphene Foam for Efficient Oil and Organic Solvent Recovery. *Small* **2015**, *11*, 5222–5229. [CrossRef] [PubMed]
13. Ge, M.; Cao, C.; Liang, F.; Liu, R.; Zhang, Y.; Zhang, W.; Zhu, T.; Yi, B.; Tang, Y.; Lai, Y. A "PDMS-in-water" emulsion enables mechanochemically robust superhydrophobic surfaces with self-healing nature. *Nanoscale Horiz.* **2020**, *5*, 65–73. [CrossRef]
14. Das, S.; Kumar, S.; Samal, S.K.; Mohanty, S.; Nayak, S.K. A Review on Superhydrophobic Polymer Nanocoatings: Recent Development and Applications. *Ind. Eng. Chem. Res.* **2018**, *57*, 2727–2745. [CrossRef]
15. England, M.W.; Urata, C.; Dunderdale, G.J.; Hozumi, A. Anti-Fogging/Self-Healing Properties of Clay-Containing Transparent Nanocomposite Thin Films. *ACS Appl. Mater. Interfaces* **2016**, *8*, 4318–4322. [CrossRef] [PubMed]

16. Isimjan, T.T.; Wang, T.; Rohani, S. A novel method to prepare superhydrophobic, UV resistance and anti-corrosion steel surface. *Chem. Eng. J.* **2012**, *210*, 182–187. [CrossRef]
17. Cao, L.; Jones, A.K.; Sikka, V.K.; Wu, J.; Gao, D. Anti-icing superhydrophobic coatings. *Langmuir* **2009**, *25*, 12444–12448. [CrossRef] [PubMed]
18. Huang, W.; Chen, Y.; Yang, C.; Situ, Y.; Huang, H. pH-driven phase separation: Simple routes for fabricating porous TiO_2 film with superhydrophilic and anti-fog properties. *Ceram. Int.* **2015**, *41*, 7573–7581. [CrossRef]
19. Han, X.; Guo, Z. Graphene and its derivative composite materials with special wettability: Potential application in oil-water separation. *Carbon* **2021**, *172*, 647–681. [CrossRef]
20. Parvate, S.; Dixit, P.; Chattopadhyay, S. Superhydrophobic Surfaces: Insights from Theory and Experiment. *J. Phys. Chem. B* **2020**, *124*, 1323–1360. [CrossRef] [PubMed]
21. Xue, C.-H.; Li, Y.-R.; Hou, J.-L.; Zhang, L.; Ma, J.-Z.; Jia, S.-T. Self-roughened superhydrophobic coatings for continuous oil–water separation. *J. Mater. Chem. A* **2015**, *3*, 10248–10253. [CrossRef]
22. Liu, Z.; Zhang, C.; Zhang, X.; Wang, C.; Liu, F.; Yuan, R.; Wang, H. Durable superhydrophobic PVDF/FEVE/GO@TiO_2 composite coating with excellent anti-scaling and UV resistance properties. *Chem. Eng. J.* **2021**, *411*, 128632. [CrossRef]
23. Zhou, H.; Wang, H.; Niu, H.; Gestos, A.; Wang, X.; Lin, T. Fluoroalkyl silane modified silicone rubber/nanoparticle composite: A super durable, robust superhydrophobic fabric coating. *Adv. Mater.* **2012**, *24*, 2409–2412. [CrossRef] [PubMed]
24. Wang, J.; Liu, X.; Jin, T.; He, H.; Liu, L. Preparation of nanocellulose and its potential in reinforced composites: A review. *J. Biomater. Sci. Polym. Ed.* **2019**, *30*, 919–946. [CrossRef] [PubMed]
25. Xu, J.; Xiang, Z.Y.; Wang, Q. Construction of PVDF/PDMS superhydrophobic surface by CNCs enhanced phase-separation. *Fine Chem.* **2023**, *40*, 2666–2675. [CrossRef]
26. Wang, L.S.; Song, T.; Cen, Y. Effects of physical properties of nanocellulose crystals on dispersion of carbon nanotubes and properties of their composite membranes. *Fine Chem.* **2025**, *42*, 332–344. [CrossRef]
27. Wenzel, R.N. Resistance of solid surfaces to wetting by water. *Ind. Eng. Chem.* **1936**, *28*, 988–994. [CrossRef]
28. Pakdel, E.; Wang, J.; Varley, R.; Wang, X. Recycled carbon fiber nonwoven functionalized with fluorine-free superhydrophobic PDMS/ZIF-8 coating for efficient oil-water separation. *J. Environ. Chem. Eng.* **2021**, *9*, 106329. [CrossRef]
29. Tan, X.; Huang, Z.; Jiang, L.; Xiao, T.; Wang, Y.; Yang, X.; Zhu, H.; Li, S.; Chen, X. A simple fabrication of superhydrophobic PVDF/SiO2 coatings and their anti-icing properties. *J. Mater. Res.* **2021**, *36*, 637–645. [CrossRef]
30. Li, C.; Liu, W.; Mao, J.; Hu, L.; Yun, Y.; Li, B. Superhydrophobic PVDF membrane modified by dopamine self-polymerized nanoparticles for vacuum membrane distillation. *Sep. Purif. Technol.* **2023**, *304*, 122182. [CrossRef]
31. Li, J.; Ren, L.-F.; Zhou, H.S.; Yang, J.; Shao, J.; He, Y. Fabrication of superhydrophobic PDTS-ZnO-PVDF membrane and its anti-wetting analysis in direct contact membrane distillation (DCMD) applications. *J. Membr. Sci.* **2021**, *620*, 118924. [CrossRef]
32. Li, J.; Ding, H.; Zhang, H.; Guo, C.; Hong, X.; Sun, L.; Ding, F. Superhydrophobic Methylated Silica Sol for Effective Oil-Water Separation. *Materials* **2020**, *13*, 842. [CrossRef] [PubMed]
33. Zhu, Y.; Pei, L.; Ambreen, J.; He, C.; Ngai, T. Facile Preparation of a Fluorine-Free, Robust, Superhydrophobic Coating through Dip Coating Combined with Non-Solvent Induced Phase Separation (Dip-Coating-NIPS) Method. *Macromol. Chem. Phys.* **2020**, *221*, 2000023. [CrossRef]
34. Xue, C.-H.; Li, X.; Jia, S.-T.; Guo, X.-J.; Li, M. Fabrication of robust superhydrophobic fabrics based on coating with PVDF/PDMS. *RSC Adv.* **2016**, *6*, 84887–84892. [CrossRef]
35. Wang, F.; Feng, L.; Li, G.; Zhai, Z.; Ma, H.; Deng, B.; Zhang, S. Fabrication and Properties of Superhydrophobic Waterborne Polyurethane Composites with Micro-Rough Surface Structure Using Electrostatic Spraying. *Polymers* **2019**, *11*, 1748. [CrossRef] [PubMed]
36. Zhang, H.; Zhang, G.; Zhu, H.; Wang, F.; Xu, G.; Shen, H.; Wang, J. Multiscale kapok/cellulose aerogels for oil absorption: The study on structure and oil absorption properties. *Ind. Crops Prod.* **2021**, *171*, 113902. [CrossRef]
37. Cao, Y.; Cheng, H.; Gu, N.; Ou, K.; Wang, Z.; Liu, Q.; Guan, R.; Fu, Q.; Sun, Y. Excellent mechanical durability of superhydrophobic coating by electrostatic spraying. *Mater. Chem. Phys.* **2023**, *301*, 127658. [CrossRef]
38. Jin, M.-Y.; Lin, Y.; Liao, Y.; Tan, C.-H.; Wang, R. Development of highly-efficient ZIF-8@PDMS/PVDF nanofibrous composite membrane for phenol removal in aqueous-aqueous membrane extractive process. *J. Membr. Sci.* **2018**, *568*, 121–133. [CrossRef]
39. Luo, Z.; Li, Y.; Duan, C.; Wang, B. Fabrication of a superhydrophobic mesh based on PDMS/SiO_2 nanoparticles/PVDF microparticles/KH-550 by one-step dip-coating method. *RSC Adv.* **2018**, *8*, 16251–16259. [CrossRef] [PubMed]
40. Li, X.; Li, J.; Gong, J.; Kuang, Y.; Mo, L.; Song, T. Cellulose nanocrystals (CNCs) with different crystalline allomorph for oil in water Pickering emulsions. *Carbohydr. Polym.* **2018**, *183*, 303–310. [CrossRef] [PubMed]
41. Guo, S.; Li, X.; Kuang, Y.; Liao, J.; Liu, K.; Li, J.; Mo, L.; He, S.; Zhu, W.; Song, J.; et al. Residual lignin in cellulose nanofibrils enhances the interfacial stabilization of Pickering emulsions. *Carbohydr. Polym.* **2021**, *253*, 117223. [CrossRef] [PubMed]

42. Guo, S.; Zhu, Y.; Xu, W.; Huan, S.; Li, J.; Song, T.; Bai, L.; Rojas, O.J. Heteroaggregation effects on Pickering stabilization using oppositely charged cellulose nanocrystal and nanochitin. *Carbohydr. Polym.* **2023**, *299*, 120154. [CrossRef] [PubMed]
43. Chen, G.; Zhang, C.; Wang, X.; Liu, H.; Guo, Y.; Qi, H. Fabrication of tailored carboxymethyl-functionalized cellulose nanofibers via chemo-mechanical process from waste cotton textile. *Cellulose* **2021**, *28*, 7663–7673. [CrossRef]
44. Wang, X.; Feng, X.; Chen, G.; Lin, B.; Qi, H. Influence of sulfation pretreatment on the structure and properties of cellulose nanofibrils. *Ind. Crops Prod.* **2022**, *187*, 115391. [CrossRef]
45. Ji, H.; Xiang, Z.; Qi, H.; Han, T.; Pranovich, A.; Song, T. Strategy towards one-step preparation of carboxylic cellulose nanocrystals and nanofibrils with high yield, carboxylation and highly stable dispersibility using innocuous citric acid. *Green Chem.* **2019**, *21*, 1956–1964. [CrossRef]
46. Luo, Y.; Song, T.; Ji, H.; Qi, H.; Xiang, Z.; Xiong, H.; Cen, Y.; Chen, G.; Han, T.; Pranovich, A. Preliminary Investigations of the Mechanisms Involved in the Ultrasonication-Assisted Production of Carboxylic Cellulose Nanocrystals with Different Structural Carboxylic Acids. *ACS Sustain. Chem. Eng.* **2021**, *9*, 4531–4542. [CrossRef]
47. Luo, J.; Song, T.; Han, T.; Qi, H.; Liu, Q.; Rosenau, T. Multifunctional roles of TEMPO-oxidized cellulose nanofibrils on the enhancement of mechanical and conductive properties of acrylic-based hydrogels for temperature response and human motion sensing. *Chem. Eng. J.* **2024**, *493*, 152649. [CrossRef]
48. Luo, J.; Song, T.; Han, T.; Qi, H.; Liu, Q.; Wang, Q.; Song, Z.; Rojas, O. Multifunctioning of carboxylic-cellulose nanocrystals on the reinforcement of compressive strength and conductivity for acrylic-based hydrogel. *Carbohydr. Polym.* **2024**, *327*, 121685. [CrossRef] [PubMed]
49. Fu, Y.; Song, T.; Tu, S.; Han, T.; Kane, A.O.; Dufresne, A. Acrylic acid-based hydrogel with multi-properties endowed by synergistic multifunction of glucurono-dialdehyde xylan and silver nanoparticles. *Int. J. Biol. Macromol.* **2026**, *362*, 152115. [CrossRef] [PubMed]
50. Song, T.; Wang, Q.; Han, T.; Dufresne, A.; da Costa, F.A.T.; Parra, D.F. Multifunctionality of carboxyl groups carried by cellulose nanocrystals for mechanical and conductive properties of acrylic-based hydrogels—Mechanism study. *Cellulose* **2025**, *32*, 10027–10049. [CrossRef]
51. Zhu, S.; Song, T.; Han, T.; Qi, H.; Liu, P.; Rosenau, T. The bifunctionality of glucurono-dialdehyde xylan (GlcU-DAX) in the preparation of silver nanoparticles with optimized size, size distribution and dispersibility: A mechanistic study. *Cellulose* **2025**, *32*, 5301–5320. [CrossRef]
52. Foorginezhad, S.; Zerafat, M.M. Fabrication of stable fluorine-free superhydrophobic fabrics for anti-adhesion and self-cleaning properties. *Appl. Surf. Sci.* **2019**, *464*, 458–471. [CrossRef]
53. Cunha, A.G.; Lundahl, M.; Ansari, M.F.; Johansson, L.S.; Campbell, J.M.; Rojas, O.J. Surface Structuring and Water Interactions of Nanocellulose Filaments Modified with Organosilanes toward Wearable Materials. *ACS Appl. Nano Mater.* **2018**, *1*, 5279–5288. [CrossRef] [PubMed]
54. Zhu, Y.; Li, H.; Huang, W.; Lai, X.; Zeng, X. Facile fabrication of superhydrophobic wood aerogel by vapor deposition method for oil-water separation. *Surf. Interfaces* **2023**, *37*, 102746. [CrossRef]
55. Liu, X.; Zhang, T.C.; He, H.; Ouyang, L.; Yuan, S. A stearic Acid/CeO_2 bilayer coating on AZ31B magnesium alloy with superhydrophobic and self-cleaning properties for corrosion inhibition. *J. Alloys Compd.* **2020**, *834*, 155210. [CrossRef]
56. He, Y.; Wang, L.; Wu, T.; Wu, Z.; Chen, Y.; Yin, K. Facile fabrication of hierarchical textures for substrate-independent and durable superhydrophobic surfaces. *Nanoscale* **2022**, *14*, 9392–9400. [CrossRef] [PubMed]
57. Deepa, B.; Abraham, E.; Cordeiro, N.; Mozetic, M.; Mathew, A.P.; Oksman, K.; Faria, M.; Thomas, S.; Pothan, L.A. Utilization of various lignocellulosic biomass for the production of nanocellulose: A comparative study. *Cellulose* **2015**, *22*, 1075–1090. [CrossRef]
58. Chu, Y.; Sun, Y.; Wu, W.; Xiao, H. Dispersion Properties of Nanocellulose: A Review. *Carbohydr. Polym.* **2020**, *250*, 116892. [CrossRef] [PubMed]
59. Rosli, N.A.; Khairudin, F.A.; Kargarzadeh, H.; Othaman, R.; Ahmad, I. Hydrophobic-oleophilic gamma-irradiated modified cellulose nanocrystal/gelatin aerogel for oil absorption. *Int. J. Biol. Macromol.* **2022**, *219*, 213–223. [CrossRef] [PubMed]
60. Lazzari, L.K.; Zampieri, V.B.; Zanini, M.; Zattera, A.J.; Baldasso, C. Sorption capacity of hydrophobic cellulose cryogels silanized by two different methods. *Cellulose* **2017**, *24*, 3421–3431. [CrossRef]
61. Kayan, A. Synthesis, Characterization, and Application of Hybrid Inorganic–Organic Composites (K/Na)ZrSi(R)Ox. *J. Inorg. Organomet. Polym. Mater.* **2016**, *26*, 640–647. [CrossRef]
62. Liang, J.; Zhou, Y.; Jiang, G.; Wang, R.; Wang, X.; Hu, R.; Xi, X. Transformation of hydrophilic cotton fabrics into superhydrophobic surfaces for oil/water separation. *J. Text. Inst.* **2013**, *104*, 305–311. [CrossRef]
63. Mahadik, S.A.; Parale, V.; Vhatkara, R.S.; Mahadik, D.B.; Kavale, M.S.; Wagh, P.B.; Gupta, S.; Gurav, J. Superhydrophobic silica coating by dip coating method. *Appl. Surf. Sci.* **2013**, *277*, 67–72. [CrossRef]

64. Baatti, A.; Erchiqui, F.; Bébin, P.; Godard, F.; Bussières, D. Fabrication of hydrophobic cellulose nanocrystals. *Can. J. Chem. Eng.* **2019**, *97*, 2050–2060. [CrossRef]
65. Guo, X.-J.; Xue, C.-H.; Sathasivam, S.; Page, K.; He, G.; Guo, J.; Promdet, P.; Heale, F.L.; Carmalt, C.J.; Parkin, I.P. Fabrication of robust superhydrophobic surfaces via aerosol-assisted CVD and thermo-triggered healing of superhydrophobicity by recovery of roughness structures. *J. Mater. Chem. A* **2019**, *7*, 17604–17612. [CrossRef]

Disclaimer/Publisher's Note: The statements, opinions and data contained in all publications are solely those of the individual author(s) and contributor(s) and not of MDPI and/or the editor(s). MDPI and/or the editor(s) disclaim responsibility for any injury to people or property resulting from any ideas, methods, instructions or products referred to in the content.